Cryogenic Milling of Titanium Powder

Jiří Kozlík [1],* [iD], **Josef Stráský** [1] [iD], **Petr Harcuba** [1] [iD], **Ilya Ibragimov** [1], **Tomáš Chráska** [2] and **Miloš Janeček** [1] [iD]

[1]   Department of Physics of Materials, Faculty of Mathematics and Physics, Charles University, 121 16 Prague, Czech Republic; josef.strasky@gmail.com (J.S.); harcuba.p@gmail.com (P.H.); ilya.ibragimov@seznam.cz (I.I.); janecek@met.mff.cuni.cz (M.J.)
[2]   Institute of Plasma Physics, Czech Academy of Sciences, 182 00 Prague, Czech Republic; chraskat@ipp.cas.cz
*   Correspondence: Jiri.Kozlik@seznam.cz; Tel.: +420-95-155-1369

Abstract: Ti Grade 2 was prepared by cryogenic attritor milling in liquid nitrogen and liquid argon. Two types of milling balls were used—stainless steel balls and heavy tungsten carbide balls. The effect of processing parameters on particle size and morphology, contamination of powder and its microhardness was investigated. Milling in liquid nitrogen was not feasible due to excessive contamination by nitrogen. Minor reduction of particle size and significant alterations in particle morphology depended on type of milling balls and application of stearic acid as processing control agent. Heavily deformed ultra-fine grained (UFG) internal microstructure of powder particles was observed by the method of "transmission Kikuchi diffraction".

1. Introduction

Titanium is a promising material for advanced applications thanks to its high specific strength, excellent corrosion resistance and good biocompatibility. In order to overcome its poor machinability and to reduce material losses, powder metallurgy routes for processing Ti and titanium alloys have been seriously considered since 1980 [1,2] and recently comprehensively reviewed in [3]. Most attention is, naturally, paid to methods of powder production and methods of subsequent compaction. However, powder metallurgy represents an opportunity to affect the properties of the final bulk material via manipulating with the powder. Characteristics of powders such as particle size, particle morphology, material contamination and internal microstructure affect the compaction processing and ultimately the properties of final bulk products.

The properties of bulk materials can be influenced by mechanical milling. The term "milling" itself obviously refers to the reduction of particle sizes by mechanical forces. However, in the case of ductile materials, the particle size reduction may not be easily achievable, which will be discussed below for titanium and its alloys. However, even when the overall particle size is reduced only slightly, internal microstructural changes within each particle might be significant. During mechanical milling, powder particles are repeatedly fragmented and cold-welded together [4], which determines their final size. However, this process is accompanied by intensive plastic deformation of individual particles and subsequent grain refinement within each of them. Note that the term "particle size" refers to the size of an individual powder particle and shall not be mixed with the term "grain size" that refers to the size of the grain of the polycrystalline structure within a particle. Finally, "crystallite size" refers to the size of a coherently diffracting domain in an X-ray diffraction (XRD) experiment.

High-energy ball milling is one of the most efficient methods for microstructural refinement of powder particles [4]. It is well known that reducing grain size in the bulk metallic material

to submicrometer levels significantly improves its mechanical properties due to the well known Hall-Petch relation. Some scientists therefore aimed on microstructural refinement via reducing the particle size of titanium powder to sub-micrometer levels by ball milling [5], despite, as described below, particle size reduction is not required for grain size reduction [6,7].

The peculiarity of titanium is an immense affinity to oxygen, nitrogen and also hydrogen intake from the environment. Ball milling of Ti in the air atmosphere resulted in formation of titanium oxides, titanium nitrides and to significant intake of O and N in hcp (hexagonal close packed) Ti-matrix [8]. The formation of uncommon fcc (face centered cubic)-Ti(O,N) was also documented [8,9]. Similarly, titanium hydride formed during ball milling of Ti in hydrogen atmosphere [10]. All these compounds and also hcp Ti-matrix with high O and/or N content are brittle and therefore allow to reduce particle size during milling. For instance, long-term milling led to particle sizes below 50 nm [5]. Despite the milling was performed in argon atmosphere, nitrogen intake could be demonstrated by observing Ti nitrides by XRD [11]. On the other hand, when the contamination by H, C, N and O was prevented, the reduction of particle sizes was only minor [12,13].

Fortunately, particle size reduction is not required for grain size reduction. High-energy ball milling provides sufficient energy to plastically deform individual powder particles. Each particle is repeatedly severely plastically deformed during the process causing an increase of dislocation density and a grain refinement. Ultra-fine grained (UFG) materials exhibit superior properties [14] and can be achieved by high-energy mechanical milling followed by appropriate compaction method [12,15,16].

Thermally activated processes of recovery and grain growth may prevent microstructural refinement by severe plastic deformation. Milling under cryogenic temperatures (typically in liquid nitrogen (LN) or liquid argon (LAr) slurry) can be employed to suppress recovery and dynamic recrystallization. Cryogenic milling leads to the reduction of powder crystallite size to the order of tens of nanometers for aluminium [7] and for titanium and its alloys [15,17,18]. At the same time, the diffusivity of possible contaminating elements such as N or O is significantly reduced [17]. Despite the reduced diffusivity, liquid nitrogen was found to be unsuitable as a cooling agent, because Ti powder became seriously contaminated by nitrogen (up to 2.99 wt % of N) even at cryogenic temperatures resulting in the brittleness of a bulk material [19]. This confirmed the earlier results obtained in [12].

Presented study shows the effect of processing parameters of cryogenic milling on particle size, morphology, microstructure, microhardness and contamination of commercially pure Ti powders. Next to commonly used stainless-steel milling balls, tungsten carbide balls were used. Hard and heavy tungsten carbide balls were successfully applied in producing titanium nitrides, borides or silicides [9,20,21]. However, the use of very hard milling medium can result in the incorporation of material of milling balls into the milled powder [4,22]. Tungsten carbide balls for milling titanium were used in a remarkable study by Sekiguchi et al. [13]. Potential contamination was avoided by covering of tungsten balls by titanium film using preliminary milling of small amount of Ti powder. Contrary to previous investigations, the presented study provides, next to other results, a direct comparison between employing stainless steel and tungsten carbide milling balls.

2. Experimental Methods

Commercially pure Ti powder (Grade 2) manufactured by gas atomization (TLS Technik GmbH & Co. Spezialpulver KG, Bitterfeld, Germany) was used as initial feedstock powder. All handling was performed in air.

Powder milling in liquid nitrogen (LN) or liquid argon (LAr) slurry (wet milling) was performed in Union Process 01-HD attritor (1400 cm^3). Stainless steel (SS) and tungsten carbide in Co matrix (WC-Co) balls (6.35 mm in diameter) were used as grinding media. WC-Co balls are significantly harder and twice heavier than SS balls, therefore an increased efficiency of milling is foreseen. Milling conditions are summarized in Table 1. Note that ball-to-powder ratio (BPR) is calculated as the ratio of mass of

balls divided by the mass of powder feed. Therefore, using high-density WC-Co balls led to doubled BPR, despite the volume of balls and the powder remained the same.

Table 1. Summary of milling process parameters. Milling time and speed for batch with WC-Co balls must have been slightly adjusted due to higher consumption of cryogenic liquid and excessive vibrations.

Sample	Cooling Liquid	Ball Material	BPR	Milling Speed (rpm)	Milling Time (h)	Stearic Acid (wt %)
LN-SS-700/4	LN	SS	16:1	700	4	–
LN-WC-650/3	LN	WC-Co	32:1	650	3.25	–
LAr-SS-700/4	LAr	SS	16:1	700	4	–
LAr-SS-700/4-SA	LAr	SS	16:1	700	4	8
LAr-WC-650/3-SA	LAr	WC-Co	32:1	650	3.25	8

Stearic acid (SA, see Table 1) was used as a process control agent to prevent excessive cold-welding in samples LAr-SS-700/4-SA and LAr-WC-650/3-SA. The used amount (8 wt % of powder) was found to be efficient in suppressing the cold-welding; it was found in a later trial attempt that 0.5 wt % might be sufficient. In order to remove remaining SA adhered to the powder particle surface after milling (and thus to reduce the overall contamination), powders were washed in ethanol and filtered using filtration paper three times.

Milled powder was observed by scanning electron microscope (SEM) FEI Quanta 200F (Hillsboro, OR, USA) equipped with a FEG (field emission gun) cathode and an EDAX energy dispersive X-ray spectroscopy (EDS) detector (Mahwah, NJ, USA). The amount of light elements (N, O, H) was measured by carrier gas hot extraction (CGHE) method. For quantitative analysis of size and morphology, powder particles were hot mounted in an epoxy resin, grinded and polished using standard metallographic methods and examined using SEM. On the cross-section of the specimen, microhardness of powders was measured by Qness Q10A testing machine (Golling, Austria) using Vickers method with very low force of 0.002 kgf (HV0.002) to reduce the size of the indent. 50 selected particles of each sample were manually measured.

In order to observe the powder internal microstructure directly, scanning electron microscopy with the detection of transmitted electrons (STEM) and transmission Kikuchi diffraction (TKD) methods were used. TKD method is also referred to as "transmission EBSD". The best planar resolution of electron back-scattered diffraction (EBSD) in conventional geometry is typically between 30 and 50 nm, and can be up to 200 nm in the perpendicular longitudinal (primary beam) direction, depending on the material and acceleration voltage [23]. For ultra-fine grained materials with grain size from few tens to hundreds of nanometers, the resolution of conventional EBSD is not sufficient since the interaction volume is comparable to the grain size. Moreover, in heavily deformed materials, the EBSD analysis is obscured by high dislocation density, residual strains and lattice rotations.

Therefore, to overcome this effect, Keller and Geiss [24] realized that Kikuchi diffraction pattern observed in common EBSD from back-scattered electrons can be observed also for forward-scattered electrons propagating through a thin sample and suggested appropriate changes in the geometry of observation. It was shown that two points with different crystalline orientation separated by only 2.5 nm [25] can be successfully measured and indexed. This method can be used in a conventional SEM equipped with an EBSD detector, nevertheless a thin specimen having the thickness of the standard TEM foil is required.

In this work, a lamella was cut from a selected powder particle and carefully thinned using gallium focused ion beam (FIB). Note that it is uneasy to find suitably oriented particle for lamella preparation and that the orientation of the lamella within the particle is unknown. Zeiss Auriga Compact FIB-SEM (Jena, Germany) with EDAX EBSD detector was used for the sample preparation, STEM imaging and TKD measurements with the step size of 5 nm. EDAX OIM software (version 7.3, Mahwah, NJ, USA, 2015) was used for data collection and processing.

3. Results

3.1. Particle Size and Morphology

Spherical morphology of the gas atomized particles (Figure 1a) was significantly changed by attritor milling to irregular shape (Figure 1b–d, SA not used) or to thin discs or plates (Figure 1e,f, SA used).
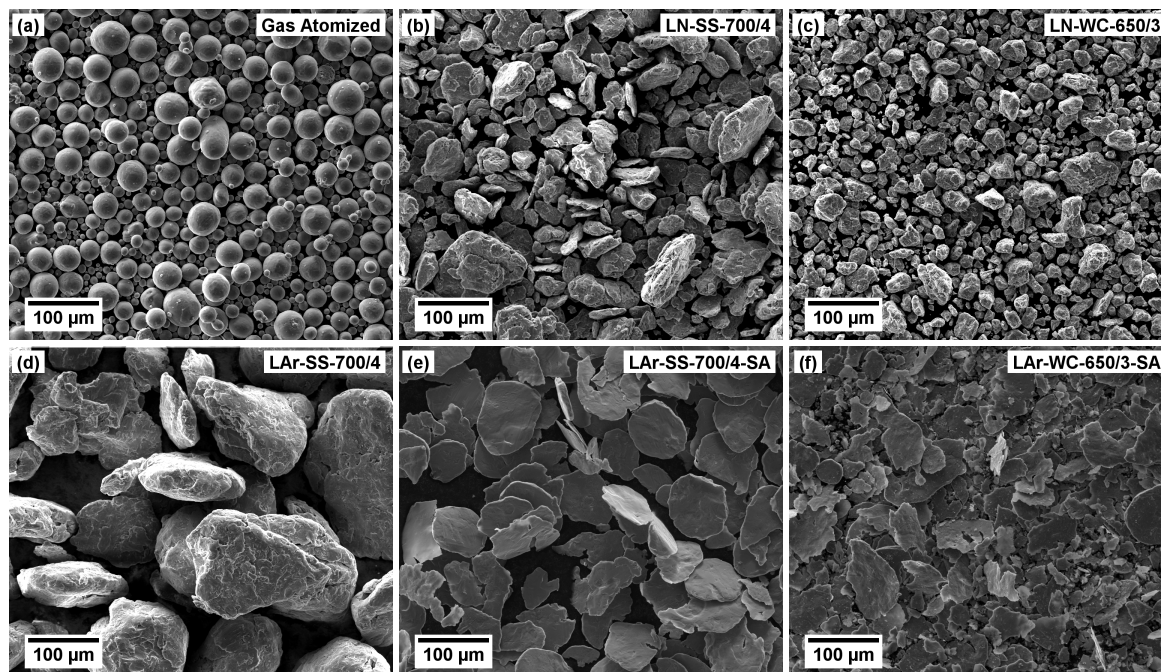

Figure 1. SEM micrographs of powders: (**a**) gas-atomized; (**b**) LN, SS balls, 4 h; (**c**) LN, WC-Co balls, 3.25 h; (**d**) LAr, SS balls, 4 h; (**e**) LAr, SS balls, 4 h, with SA; (**f**) LAr, WC-Co balls, 3.25 h, with SA.

Due to significantly different shapes of powder particles, it is not obvious how to determine and compare particles sizes. Maximum and minimum Feret diameter (also known as caliper diameter) and their ratio (aspect ratio) was evaluated for each particle from cross-section images (several thousand of particles were analyzed for each sample). The median, 10th and 90th percentile (weighted by relative area) were calculated, the results are summarized in Table 2. Cryogenic milling lead to minor particle size reduction only when cold-welding was suppressed, while morphology was significantly affected in all samples as documented by Figure 1.

Table 2. Particle size and shape characteristics. The median d_{50}, 10th and 90th percentile d_{10} and d_{90} of Feret diameter and the median of aspect ratio a_{50} are given for each sample.

Sample	Feret Diameter (µm)						Aspect Ratio
	Max.			Min.			
	d_{10}	d_{50}	d_{90}	d_{10}	d_{50}	d_{90}	a_{50}
gas atomized	22	37	49	16	30	41	1.22
LN-SS-700/4	30	75	150	15	43	93	1.71
LN-WC-650/3	18	43	87	11	27	54	1.55
LAr-SS-700/4	110	160	250	54	110	170	1.52
LAr-SS-700/4-SA	31	74	150	8	19	74	3.47
LAr-WC-650/3-SA	13	38	81	3	7	17	5.60

Particles in powders milled without stearic acid clearly formed by excessive cold-welding of deformed and fragmented particles. This is particularly seen in Figure 2d, where elongated pore chains

form a splat-like internal structure of particles with elongated pores and cracks. Particles of powder milled in liquid argon without the use of stearic acid (sample LAr-SS-700/4) are significantly larger than initial gas-atomized particles (see Figure 1a,d) suggesting that process of cold-welding is faster than the process of fragmentation which may not occur at all.
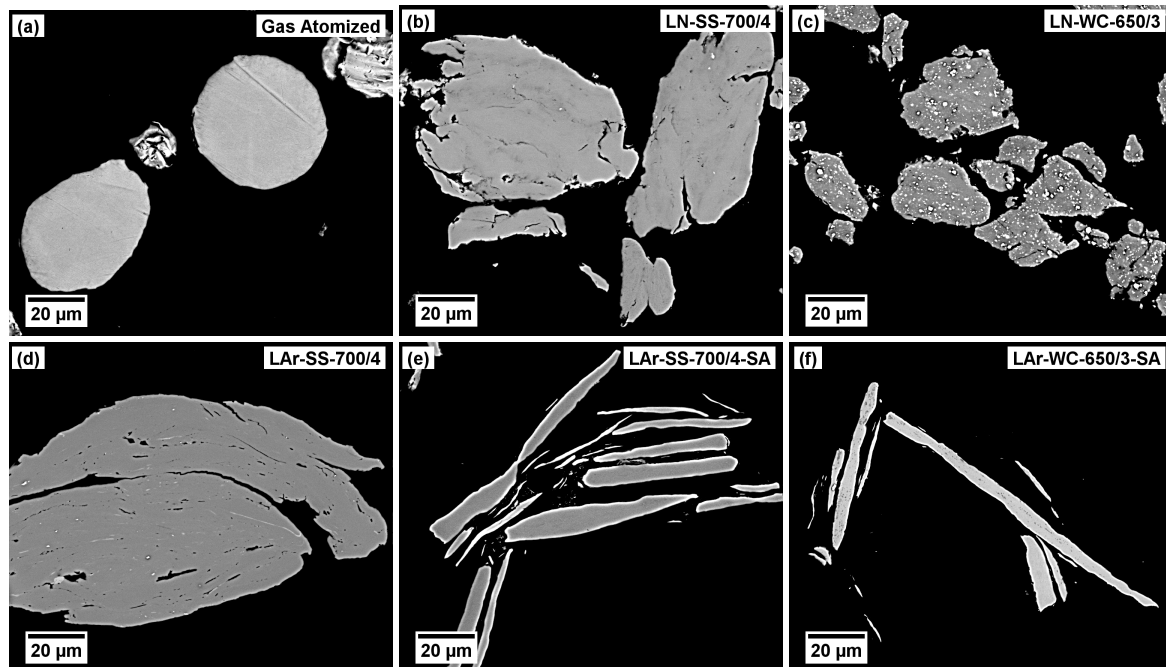

Figure 2. SEM micrographs of powder cross-sections: (**a**) gas-atomized; (**b**) LN, SS balls, 4 h; (**c**) LN, WC-Co balls, 3.25 h; (**d**) LAr, SS balls, 4 h; (**e**) LAr, SS balls, 4 h, with SA; (**f**) LAr, WC-Co balls, 3.25 h, with SA.

Particles of powders milled in liquid nitrogen (sample LN-SS-700/4 and especially sample LN-WC-650/3) are significantly smaller than sample LAr-SS-700/4 milled in liquid argon without SA, which might be connected to increased brittleness due to nitrogen contamination. Cold-welding is, nevertheless, present also in these conditions as illustrated in Figure 2b,c.

On the other hand, stearic acid prevented cold-welding of particles. Each particle is repetitively deformed by compression and attrition forces resulting in flat and disc-shaped particles (Figure 1e). Utilizing WC-Co balls (Figure 1f) increased the intensity of milling and disc-shaped particles become thinner and their average volume is significantly lower. It is, therefore, suggested that thin discs fragmented during milling into smaller flat particles.

3.2. Microstructure and Transmission Kikuchi Diffraction

The sample milled in liquid argon LAr using stainless steel balls and with the use of stearic acid (sample LAr-SS-700/4-SA) was investigated in more detail. Conventional SEM and EBSD observations failed due to the small grain size of the powder particles.

STEM and TKD observations of the specimens were capable to visualize the refined structure. The lamella for microstructure investigation was cut directly from the powder embedded in an epoxy resin using FIB (focused ion beam) milling as illustrated in Figure 3. The lamella was cut approximately parallel to the longitudinal direction of the particle visible on the cross-section surface. However, the exact orientation of the lamella with respect to the disc-shaped particle is unknown as the particle may not be mounted exactly perpendicularly to the cross-section surface. The misorientation between lamella and the particle can be up to 30°.
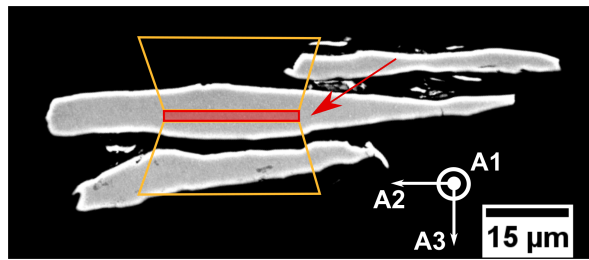
Figure 3. Cross-section view of powder particles with denoted cuts for the lamella preparation. Red—the lamella, orange—trenches for lamella lift-out. The axes A1–A3 correspond to the axes in pole figures in Figure 5.

After cutting and lift-out of the lamella, central part of the lamella was carefully thinned by FIB using decreasing ion current.

The microstructure was observed using STEM detector in SEM at 30 kV as shown in Figure 4. The heavily deformed microstructure with sub-grain sizes around 100 nm was observed. Note that the contrast in the Figure 4 is similar to diffraction contrast in TEM and sub-grains cannot be unambiguously distinguished from grains. Therefore, transmission Kikuchi diffraction (TKD) was performed to determine the grain orientation relationships and consequently the true grain structure of milled powder.
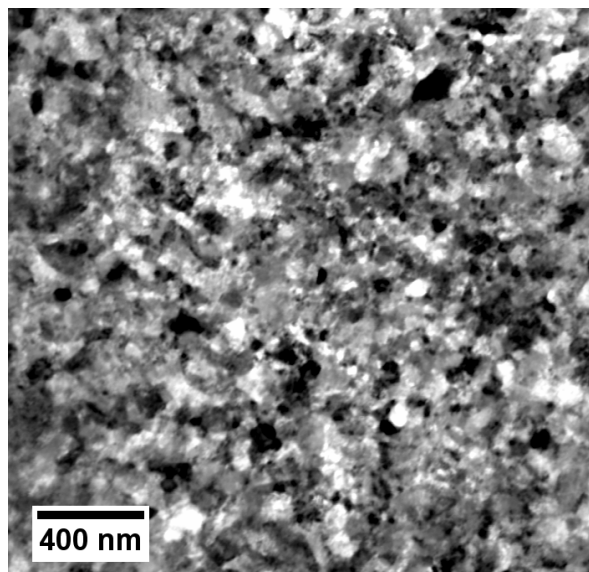

Figure 4. Orientation dark-field STEM image showing the microstructure of sample LAr-SS-700/4-SA.

Figure 5 shows the inverse pole figure map (IPF map) of the TKD. The grain size observed in IPF map is in the range of 30–300 nm with the area weighed mean value of 110 nm. It can be also seen that the grains are mostly separated by high angle grain boundaries (HAGB) with lattice misorientation >15°.

TKD mapping also revealed texture with <0001> directions tilted 30–40° from the A1–A3 plane. Note that the rotation along A2 axis cannot be precisely determined, because orientation of the lamella with respect to the original particle is not known.
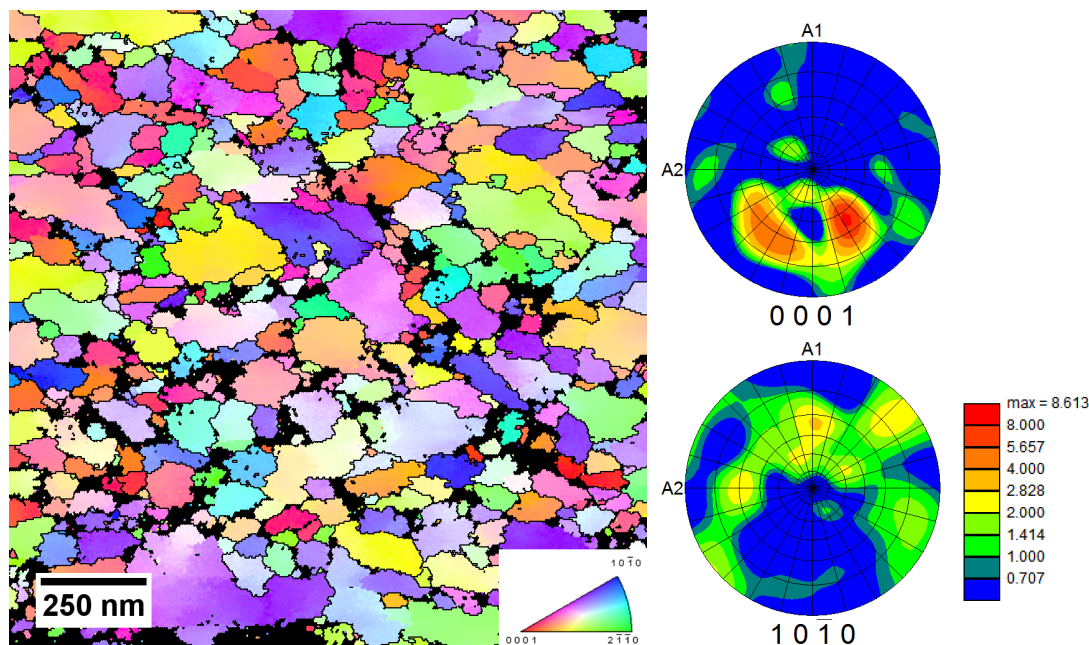
Figure 5. IPF map and corresponding pole figures of a milled powder sample. Scanned area 1.5 μm × 1.5 μm, step size 5 nm, only well indexed points are shown. High angle grain boundaries (>15°) are marked by black lines. The axes A1 and A2 in the pole figures correspond to the axes shown in Figure 3.

3.3. Contamination

Two types of contamination are usually involved in milled Ti—contamination from milling environment, namely process control agent (SA), atmosphere or cooling liquid (H, C, N, O), and contamination from balls and milling tank (Fe, WC-Co). The contamination by hydrogen, nitrogen and oxygen was measured by CGHE method and the results are summarized in Table 3.

Table 3. Contamination of cleaned powders by carrier gas hot extraction (CGHE) analysis (estimated relative error 5%) and Vickers microhardness (HV0.002) of powder particles measured on the cross-section.

Sample	Hydrogen (wt %)	Nitrogen (wt %)	Oxygen (wt %)	HV0.002
gas atomized	0	0.02	0.15	239 ± 30
LN-SS-700/4	0	0.80	0.43	390 ± 42
LN-WC-650/3	0	2.99	0.36	484 ± 66
LAr-SS-700/4	0	0.20	0.23	456 ± 31
LAr-SS-700/4-SA	0.05	0.06	0.36	327 ± 31
LAr-WC-650/3-SA	0.03	0.08	0.59	315 ± 61

Hydrogen contamination was detected only in powders milled with SA as the process control agent. Concentration of nitrogen depends on the milling environment (LN vs. LAr), material of milling balls (i.e., the intensity of milling) and application of stearic acid. Milling in liquid nitrogen led to excessive nitrogen contamination exceeding 0.5 wt %. Nitrogen contamination was observed also after milling in liquid argon and could be reduced by utilization of stearic acid. Oxygen contamination is also substantial and seems to be rather independent of milling environment, milling intensity and application of stearic acid.

Area EDS analysis was performed on a particle cross-section to determine the concentration of heavier elements. Trace amount of Fe (0.5 wt % max.) was detected in all samples including the initial

one and differences between samples were not detected. It indicates that Fe contamination in the gas atomized material, which is common in commercial purity Ti, did not increase during milling. The contamination of powder by iron from milling tank, shaft and stainless steel balls was therefore only limited.

On the other hand, small WC-Co particles (approximately 1 μm in diameter) were observed inside Ti particles milled in liquid nitrogen (sample LN-WC-650/3, Figure 6a) and on the particle surface of powder milled in liquid argon with the use of stearic acid (sample LAr-WC-650/3-SA, Figure 6b). In both cases, small WC-Co particles are fragments of grinding balls which became considerably brittle under low temperatures. In the sample LAr-WC-650/3-SA, no WC-Co particles were found within particle interior (investigated on cross-sections, Figure 2f). This is attributed to the use of stearic acid, which prevents cold-welding of Ti particles, unlike in the sample LN-WC-650/3, where WC-Co particles are trapped in Ti particle interior by repetitive cold-welding.
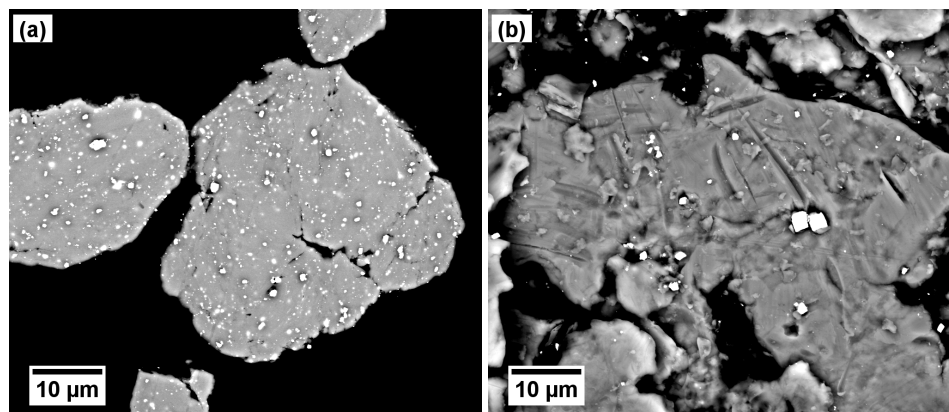

Figure 6. WC-Co seen as bright spots (back-scattered electron contrast): (**a**) inside Ti particles; (**b**) on the particle surface.

3.4. Microhardness

The results of microhardness measurements are shown in the very right column of Table 3. The measurement was accompanied by several difficulties. Very low load of 0.002 kgf was applied to fit the indent within the particle interior. Evaluation of size of such small indents is imprecise which leads to high standard deviation of measured HV values. Finally, the measurement showed, that the hardness among particles of powders milled without the use of stearic acid is not fully homogeneous. In the sample LN-WC-650/3, indents near WC-Co particles were avoided.

It can be seen in Table 3 that microhardness significantly increases with increasing nitrogen content. In samples LAr-SS-700/4-SA and LAr-WC-650/3-SA, the contamination by nitrogen is limited and increased microhardness can be attributed to increased oxygen content and also microstructural refinement.

4. Discussion

4.1. Particle Size

Ti powder particles were not significantly fragmented by high-energy ball milling even at cryogenic temperatures. It is well known that α-Ti with low content of impurities remain ductile at cryogenic temperatures [26] as in the case of powders milled in LAr. Significant reduction of Ti powder particle sizes (to submicrometer level) was achieved only for contaminated powders [5], such as powders milled in LN.

4.2. Microstructure

Milled powder observed by transmission Kikuchi diffraction exhibits ultra-fine grained structure with typical grain size of approximately 100 nm and high volume fraction of high-angle grain boundaries. Such structure is comparable to UFG Ti prepared by severe plastic deformation, namely by equal channel angular pressing (ECAP) [27] and high pressure torsion (HPT) [28]. It is, therefore, confirmed that deformation of particles during high-energy milling is qualitatively comparable to severe plastic deformation of bulk material.

TEM observations in [13] revealed similar ultra-fine grained structure in the heavily deformed shell (area in the vicinity of particle edge) of comparatively large and relatively round particles. However, using stearic acid in our study leads to the formation of smaller flat disc-shaped particles and equiaxed UFG structure inside the particles. However, planetary mill used in [13] leads to deformation mainly by compression between a ball and milling tank, while milling in so-called attritor mill causes deformation of a particle powder predominantly by attrition forces (shear) between two milling balls. The BPR (and therefore milling intensity) in [13] is also significantly lower than in this study (1.8:1 vs. 16:1 or 32:1), therefore the results cannot be quantitatively compared. As the result, particular effect of cryogenic temperature on microstructural refinement of Ti cannot be so far established and constitutes an interesting research issue for future investigation.

For the subsequent compaction (for instance by sintering techniques), the particle shape is not critical. However, the disc-shaped particles after milling with the use of SA would not be oriented randomly during compaction and consequently prevailing crystallographic texture within the particles could be transmitted to the bulk material. On the other hand, there are methods (for example selective laser melting), where good powder flowability is required for proper formation of powder layer. Atomized powders with spherical particles are therefore more suitable for this family of methods.

4.3. Texture

The texture observed in the prepared lamella as shown in Figure 5 originates by the nature of a milling process, where two dominating deformation mechanisms are involved: compression and shear in the particle plane. These deformation modes are very similar to those during rolling. Indeed, the observed texture is very similar to rolling texture in Ti, where <0001> poles are tilted by 30–40° from the normal towards transverse direction and <10$\bar{1}$0> poles pointing towards the rolling direction [29], which is caused by the preferential activation of specific slip systems. Note that texture was determined with respect to the lamella surface, while particle plane might be slightly tilted, which accounts for differences between typical rolling texture and the observed texture.

4.4. Contamination

Contamination is an inevitable problem of powder metallurgy and mechanical milling in particular due to large surface area of particles and formation of new surfaces during process. Contamination by Fe from stainless steel milling balls and milling tank was found insignificant, while contamination by H, N and O is critical.

Hydrogen contamination is related only to the use of stearic acid. Powder milled with stearic acid was cleaned by ethanol and during cleaning the contamination by hydrogen was reduced from approximately 1 wt % (not shown in results) to 0.03–0.05 wt % (see Table 3). It is, therefore, assumed that hydrogen is bonded in stearic acid even after milling and the cleaning procedure is efficient in removing excessive stearic acid. There are no signs of formation of titanium hydrides [10], however, this eventuality cannot be ruled out. The stearic acid has only a minor effect as a source of oxygen contamination, since the oxygen content in the SA molecule is low.

There is always some oxygen and nitrogen present in the liquid argon, since it is produced by the fractional distillation of liquid air. The cryogenic liquid is therefore supposed to be the major source of contamination by O and N. Stearic acid prevents cold-welding of particles and may act as

a protective film on a particle surface preventing nitrogen trapping. The overall contamination as measured by CGHE might be therefore higher in powders with larger relative surface area (namely for disc-shaped particles) due to contamination of surface of particles. This hypothesis is consistent with increased nitrogen and oxygen contamination in samples milled in liquid argon with the use of stearic acid (samples LAr-SS-700/4-SA and LAr-WC-650/3-SA). Note that the true contamination of particles interior could be lower than the overall contamination measured by CGHE method.

The measured nitrogen contamination is significantly lower than reported by Ertorer et al. [12] (0.59 wt % of N) after 8 h of milling in LAr. This may be caused by longer milling duration and different purity of cooling liquid.

4.5. Microhardness

Hardness of the Ti powder is influenced mainly by increased concentration of interstitials (namely N and O) and by the microstructural refinement. Nonetheless, the actual measured microhardness values might have been affected by the size of the powder particles. The distance of the indent from the edge of the particle was small and could not meet the technical standards for microhardness measurements of bulk samples. As the result, the measured HV values might be smaller than the true hardness, especially in the case of powders with smaller (flat) particles.

All milled powders showed higher microhardness when compared to the initial gas-atomized powder. Microhardness increase in powders milled in liquid nitrogen can be fully attributed to nitrogen contamination. Surprisingly high microhardness of samples milled in LAr without stearic acid (sample LAr-SS-700/4) can be attributed to grain refinement, nitrogen and oxygen contamination inside the particles and also to the fact that this powder was composed of biggest particles. On the other hand, particles of powders milled with the use of stearic acid (samples LAr-SS-700/4-SA and LAr-WC-650/3-SA) are thin and the microhardness might be underestimated. Despite of that, microhardness increased from the gas-atomized condition. It is assumed that since stearic acid avoided cold-welding, the contamination by oxygen and nitrogen is present predominantly at the particles surface. Therefore, the observed hardening can be mostly attributed to the microstructure refinement, which is consistent with results in [30].

However, precise determination of the effect of microstructural refinement on the hardness would require utilization of nano-indentation technique and detail monitoring of spatial distribution of contaminants, which is beyond the scope of this study.

5. Conclusions

Commercially pure titanium powder was processed by cryogenic milling. It can be concluded that:

- Ti powder particle size was reduced by cryogenic milling in LN and LAr only at certain processing conditions when cold-welding was avoided.
- Transmission Kikuchi Diffraction (TKD) proved that high-energy attritor milling is capable of forming ultra-fine grained microstructure with grain size of approximately 100 nm and high fraction of high angle boundaries.
- Milling in liquid nitrogen results in severe contamination of Ti powder by nitrogen.
- Stearic acid as process control agent prevents the cold-welding during milling. Powder particles changed shape from spherical to disc/plate-shaped particles.
- Milling with WC-Co balls leads to contamination by tungsten carbide particles.
- Texture of disc-shaped particles is similar to the typical rolling texture of Ti.
- Microhardness of all samples increased after milling as a result of contamination by nitrogen and oxygen and due to the dislocation/grain boundary strengthening.

References

1. Froes, F.H.; Smugeresky, J.E. *Powder Metallurgy of Titanium Alloys: Proceedings of a Symposium*; Metallurgical Society of AIME: Warrendale, PA, USA, 1980.
2. Froes, F.H.; Eylon, D.; Eichelman, G.E.; Burte, H.M. Developments in titanium powder metallurgy. *J. Microsc.* **1980**, *32*, 47–54.
3. Qian, M.; Froes, F.H. *Titanium Powder Metallurgy*; Elsevier: Amsterdam, The Netherlands, 2015.
4. Suryanarayana, C. Mechanical alloying and milling. *Prog. Mater. Sci.* **2001**, *46*, 1–184.
5. Dabhade, V.V.; Rama Mohan, T.R.; Ramakrishnan, P. Nanocrystalline titanium powders by high energy attrition milling. *Powder Technol.* **2007**, *171*, 177–183.
6. Fecht, H.J. Nanostructure formation by mechanical attrition. *Nanostruct. Mater.* **1995**, *6*, 33–42.
7. Witkin, D.B.; Lavernia, E.J. Synthesis and mechanical behavior of nanostructured materials via cryomilling. *Prog. Mater. Sci.* **2006**, *51*, 1–60.
8. Lu, C.J.; Zhang, J.; Li, Z.Q. Structural evolution of titanium powder during ball milling in different atmospheres. *J. Alloys Compd.* **2004**, *381*, 278–283.
9. Yang, H.; McCormick, P.G. Synthesis of titanium oxynitride by mechanical milling. *J. Mater. Sci.* **1993**, *28*, 5663–5667.
10. Zhang, H.; Kisi, E.H. Formation of titanium hydride at room temperature by ball milling. *J. Phys.* **1997**, *9*, L185.
11. Dabhade, V.V.; Rama Mohan, T.R.; Ramakrishnan, P. Synthesis of nanosized titanium powder by high energy milling. *Appl. Surf. Sci.* **2001**, *182*, 390–393.
12. Ertorer, O.; Zúñiga, A.; Topping, T.; Moss, W.; Lavernia, E.J. Mechanical behavior of cryomilled CP-Ti consoliyeard via quasi-isostatic forging. *Metall. Mater. Trans. A* **2008**, *40*, 91–103.
13. Sekiguchi, T.; Ono, K.; Fujiwara, H.; Ameyama, K. New microstructure design for commercially pure titanium with outstanding mechanical properties by mechanical milling and hot roll sintering. *Mater. Trans.* **2010**, *51*, 39–45.
14. Langdon, T.G. Twenty-five years of ultrafine-grained materials: Achieving exceptional properties through grain refinement. *Acta Mater.* **2013**, *61*, 7035–7059.
15. Ertorer, O.; Topping, T.; Li, Y.; Moss, W.; Lavernia, E.J. Enhanced tensile strength and high ductility in cryomilled commercially pure titanium. *Scr. Mater.* **2009**, *60*, 586–589.
16. Ertorer, O.; Topping, T.D.; Li, Y.; Moss, W.; Lavernia, E.J. Nanostructured Ti consoliyeard via spark plasma sintering. *Metall. Mater. Trans. A* **2011**, *42*, 964–973.
17. Sun, F.; Rojas, P.; Zúñiga, A.; Lavernia, E.J. Nanostructure in a Ti alloy processed using a cryomilling technique. *Mater. Sci. Eng. A* **2006**, *430*, 90–97.
18. Dheda, S.S.; Melnyk, C.; Mohamed, F.A. Effect of titanium nitride nanoparticles on grain size stabilization and consolidation of cryomilled titanium. *Mater. Sci. Eng. A* **2013**, *584*, 88–96.
19. Kozlik, J.; Becker, H.; Strasky, J.; Harcuba, P.; Janecek, M. Influence of milling parameters on particle size and microhardness of cryomilled and spark plasma sintered CP Ti. In Proceedings of the Metal 2016: 25th Anniversary International Conference on Metallurgy and Materials, Brno, Czech Republic, 25–27 May 2016; pp. 1439–1444.
20. Kudaka, K.; Iizumi, K.; Sasaku, T. Mechanochemical syntheses of titanium carbide, diboride and nitride. *J. Ceram. Soc. Jpn.* **1999**, *107*, 1019–1024.
21. Kudaka, K.; Iizumi, K.; Sasaki, T.; Izumi, H. Effect of milling media on the reactionkinetics of the mechanochemical synthesis of pentatitanium trisilicide. *J. Am. Ceram. Soc.* **2000**, *83*, 2887–2889.

22. Haruyama, O.; Asahi, N. Amorphization of Mixed Ni and Zr Powders by Mechanical Alloying. *Mater. Sci. Forum* **1992**, *88*, 333–338.

23. Chen, D.; Kuo, J.C.; Wu, W.T. Effect of microscopic parameters on EBSD spatial resolution. *Ultramicroscopy* **2011**, *111*, 1488–1494.

24. Keller, R.; Geiss, R. Transmission EBSD from 10 nm domains in a scanning electron microscope. *J. Microsc.* **2012**, *245*, 245–251.

25. De Kloe, R. Transmission-EBSD—Taking Transparency to a New Level. 2014. Available online: https://edaxblog.com/2014/10/02/transmisson-ebsd-taking-transparency-to-a-new-level/ (accessed on 27 November 2017).

26. Hurlich, A.; Watson, J.F. Selection of Materials for use at cryogenic temperatures. *Met. Prog.* **1961**, *79*, 65–72.

27. Stolyarov, V.V.; Zhu, Y.T.; Alexandrov, I.V.; Lowe, T.C.; Valiev, R.Z. Influence of ECAP routes on the microstructure and properties of pure Ti. *Mater. Sci. Eng. A* **2001**, *299*, 59–67.

28. Sergueeva, A.V.; Stolyarov, V.V.; Valiev, R.Z.; Mukherjee, A.K. Advanced mechanical properties of pure titanium with ultrafine grained structure. *Scr. Mater.* **2001**, *45*, 747–752.

29. Wang, Y.N.; Huang, J.C. Texture analysis in hexagonal materials. *Mater. Chem. Phys.* **2003**, *81*, 11–26.

30. Václavová, K.; Stráský, J.; Polyakova, V.; Stráská, J.; Nejezchlebová, J.; Seiner, H.; Semenova, I.; Janeček, M. Microhardness and microstructure evolution of ultra-fine grained Ti-15Mo and TIMETAL LCB alloys prepared by high pressure torsion. *Mater. Sci. Eng. A* **2017**, *682*, 220–228.